International Journal for Housing Science and Its Applications
Publish August 6, 2025. Volume 46, Issue 3 Pages 5019-5031

https://doi.org/10.70517/ijhsa463430

Assessment method of supply and demand risk adjustment capacity of provincial power grid with high proportion of new energy based on multidimensional spatio-temporal computational modeling

Fangzhao Deng[1], Zhenli Deng[1,*], Boning Yu[1] and Xiaoliang Jiang[1]
[1] State Grid Henan Economic Research Institute, Zhengzhou, Henan, 450000, China
Corresponding authors: (e-mail: DengzZli@163.com).

Abstract This paper takes the multi-energy microgrid, an important part of the grid regulation capability, as the entry point, and designs the energy input model and the energy interaction model successively based on the storage mode of the multi-energy microgrid supply. The two models are used to analyze the energy conversion and input-output relationship between energy sources, and to establish a multi-energy microgrid power regulation model. Subsequently, the inertia change rate index is proposed to analyze and extract the time-varying characteristics of the inertia of the new energy grid system as a method to judge the trend of the inertia level change of the grid system. At the same time, considering that the grid system needs to consume the adjustable resource participation capacity to deal with internal operation problems, the evaluation method of external participation capacity is built by partitioning the grid into networks. Combining the above, an assessment method of the supply and demand risk adjustment capacity of the provincial grid system with high proportion of new energy is formed. The method is used to analyze the regulating ability of energy storage units in the grid system, and further proposes four indicators for assessing the potential regulating ability of the grid system: outputable power (Eout), inputable power (Ein), maximum abandoned power (Eg), and maximum load shedding power (EL). Based on the four assessment indexes, the assessment method in this paper calculates the difference between the theoretically calculated value of the outputable power (Eout) and the inputable power (Ein) and the simulation results are less than or equal to 0.00 as a negative value in simulation experiments, which verifies that the theoretical value is that the microgrid can be ensured to provide or absorb power to the outside world in the next cycle.

Index Terms supply and demand risk regulation, microgrid power regulation model, inertia time-varying characteristics, new energy grid system

I. Introduction

With China's development plan and a series of preferential incentives for the continuous implementation of policies to strengthen the construction of wind power and photovoltaic power generation projects, while guaranteeing the mechanism of power delivery and consumption, and improving the competitiveness of the market, to promote the wind power and photovoltaic power generation projects have entered a new stage of high-quality development [1]-[4]. Currently, China's installed capacity of wind power and photovoltaic power generation accounts for about more than 20% of the total power supply capacity, and new energy has become the second largest power source in China [5], [6]. The rapid development of new energy represented by wind power and photovoltaic continues to form a high proportion of new energy power systems within China, and the proportion of new energy power generation capacity in the power system is increasing, and its impact on the safe, reliable and stable operation of the power system is becoming more and more significant [7]-[10].

With the interconnection of the grid scale and the diversification of power loads, the problem of grid operation security and stability is becoming more and more prominent, and the large-scale access of new energy sources such as wind and light has further aggravated the strong uncertainty of grid operation security and has brought a great test to the safe, stable and reliable operation of the power grid [11]-[14]. In the context of a high proportion of new energy, the supply and demand risk regulation of the provincial power grid faces a number of challenges [15]. The first is the volatility of electricity demand [16]. With the development of social economy and the improvement of people's living standard, the demand for electricity is growing, and the change of demand has uncertainty [17], [18]. Secondly, it is the instability of new energy [19]. With the promotion and application of clean energy, the access to

new energy sources such as wind and solar energy has grown exponentially [20]. However, the instability of these new energy sources brings challenges to the scheduling and supply-demand balance of the power system [21], [22]. Again, it is the security of the power system [23]. The security of power system operation is the basis of power supply and demand balance, and any unexpected events will bring unpredictable risks to the power system [24], [25]. Based on this, it is of major significance to assess the supply and demand risk adjustment ability of provincial power grids with high proportion of new energy sources to take effective measures to promote the balance of power supply and demand.

This paper firstly explains the construction method and operation principle of the energy input model and energy interaction model to form a multi-energy microgrid power regulation model. Secondly, it analyzes the calculation process of inertia rate of change index, analyzes and extracts the time-varying characteristics of inertia of new energy grid system, and then identifies the trend of inertia level of the grid system. In the form of network partitioning, we also propose a method for assessing the external net participation capacity, so as to solve the loss of the participation capacity of adjustable resources in the grid system due to the handling of internal operation problems. Preliminarily, the assessment method of the grid system's supply and demand risk adjustment capacity is formed. The key indexes of adjustable load regulation capability are examined and the power load trend is analyzed to verify the effectiveness of the assessment method, taking the cross-provincial power grid system in Southwest China as an experimental object. Finally, by analyzing the regulation capability of microgrid energy storage units, the theoretical calculation of potential regulation capability during the scheduling period and simulation operation simulation are carried out to further propose the assessment indexes of potential regulation capability of the power grid system.

II. Assessment of the ability of the grid system to regulate supply and demand risks

II. A. Multi-energy microgrid power regulation modeling

II. A. 1) Energy input modeling

(1) Superior grid model

The power supply of the multi-energy microgrid is mainly divided into two parts: internal supply by gas turbines, fuel cells and distributed power sources. The external supply of power is supplemented by the purchase and sale of power from the grid to ensure a stable supply of power. Although the distributed power generation in the microgrid also exists in the fluctuation of power, but multi-energy by virtue of its own multi-energy coupling, the microgrid can meet its own needs at the same time, the energy surplus for the grid to provide regulation. Especially when the power fluctuation of renewable energy in the power grid, so that the regulating unit needs to constantly adjust the unit power. In order to respond to the demand for regulation, the multi-energy microgrid absorbs and discharges energy by increasing or decreasing the output of each unit. Therefore, the multi-energy microgrid connects the microgrid to the grid through the purchase and sale of electricity, and responds to the grid regulation demand through the combination of units between the energy conversion device and the power supply unit in the microgrid.

Multi-energy microgrid has a strong energy regulation capability by virtue of multi-energy conversion and storage, which can assist the higher-level grid in power supply and consumption while ensuring the balance of power supply and demand in the microgrid. When there is a power shortage in the higher-level grid, the multi-energy microgrid can purchase and sell power from the higher-level grid to assist the stable operation of the grid. However, the purchased and sold power is related to the size of the microgrid's own regulation capacity and the power of the contact line. Therefore, the interaction power of the two should be within the limits of its own regulation range and contact line power. They are shown in equations (1)-(3):

$$\sum_{t=1}^{T}\left(P_{E,in}^{t}+P_{DP}^{t}\right)=\sum_{t=1}^{T}\left(P_{E,out}^{t}+L_{E}^{t}\right) \tag{1}$$

$$0\le\sum_{t=1}^{T}P_{E,out}^{t}\le\sum_{t=1}^{T}P_{E,out,\max}^{t} \tag{2}$$

$$\left|P_{E,out}^{t}-P_{E,out}^{t-1}\right|\le E_{u}^{t}\Delta t \tag{3}$$

where $P_{E,in}^{t}$ is the purchased power, $P_{E,out}^{t}$ is the outgoing power, P_{DP}^{t} the distributed power output, and L_{E}^{t} is the load power. $P_{E,out,\max}^{t}$ is the upper limit of transmission capacity and E_{u}^{t} is the creepage parameter of electric power, respectively.

(2) Natural gas network model

As an important source of gas energy for microgrid, natural gas is mainly supplied to gas turbines, which are cleaner and more efficient than traditional thermal power units. The gas turbine not only serves as a power supply unit, but also recycles heat energy through the waste heat device. The supply of gas to the microgrid comes from the external gas grid, which is connected to the pipeline to purchase energy. The gas balance constraint of the multi-energy microgrid should not exceed the upper limit value of the gas power supplied by the contact pipeline when purchasing gas, as shown in equation (4).

$$0 \le P_{G,in}^{t} \le P_{G,in,\max}^{t} \tag{4}$$

where $P_{G,in}^{t}$ is the purchased gas power external to the multi-energy microgrid at time t, and $P_{G,in,\max}^{t}$ is the maximum value of the supplied gas power of the gas network at time t.

II. A. 2) Energy interaction models

The energy interaction hub can be abstracted as an input-output port model: for any multi-energy microgrid, it can be abstracted into the form of raw input energy, which is eventually transformed into output energy. The Energy Interaction Hub is illustrated in Figure 1 and contains three main types of devices: energy transmission devices, such as electricity, natural gas and heat networks. Energy conversion devices, that is, a form of energy into another form of energy devices, such as gas - electricity, electricity - heat and electricity - gas and other equipment. Energy storage devices, such as heat storage, gas storage and other devices.

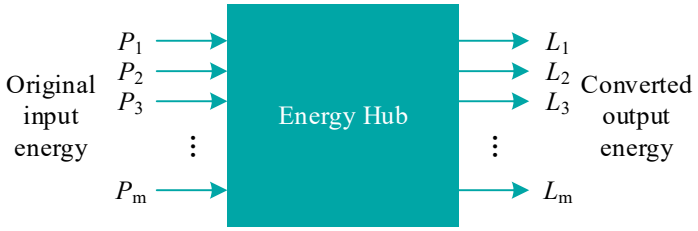

Figure 1: Energy interaction hub

Assuming m energy sources at the input and n energy sources at the output, the energy coupling model can be described by the mathematical model of equation (5):

$$\begin{bmatrix} L_1 \\ L_2 \\ \vdots \\ L_n \end{bmatrix} = \begin{bmatrix} c_{11} & c_{12} & \cdots & c_{1m} \\ c_{21} & c_{22} & \cdots & c_{2m} \\ \vdots & \vdots & \ddots & \vdots \\ c_{n1} & c_{n2} & \cdots & c_{nm} \end{bmatrix} \begin{bmatrix} P_1 \\ P_2 \\ \vdots \\ P_m \end{bmatrix} \tag{5}$$

The energy coupling model is established according to the energy interaction hub as Eq. (5), and this matrix form is adopted to represent the multi-energy microgrid.

The energy storage and hydrogen energy conversion vectors are taken into account in Eq. (5), and the model is improved by introducing modifications to obtain Eq. (6). For the multi-energy microgrid steady state study, without considering the losses on the line, there is a power limitation on the raw input energy as shown in Eq. (7):

$$L + S = CP + A \tag{6}$$

$$P^{\min} \le P \le P^{\max} \tag{7}$$

where C is the energy conversion matrix between multiple energy sources. P is the original input vector. L is the load vector in the microgrid. S is the energy storage vector. A is the energy supply vector. For microgrids, the introduction of correction quantities allows for a clearer representation of the form of energy conversion. First, the following microgrid input-output vectors and energy storage-supply vectors are introduced as Eqs. (8)-(11):

$$P = \left[\Delta P_E + P_{DP}, P_{Gas}\right]^T \tag{8}$$

$$L = \left[L_E, L_T, L_H, L_G\right]^T \tag{9}$$

$$S=\left[0,S_T,S_H,0\right]^T \tag{10}$$

$$A=\left[P_{fc}^E,0,0,P_{Gas}^M\right]^T \tag{11}$$

where P_{DP} is the distributed generation equipment output in the microgrid, and ΔP_E is the difference between the input and output electric power of the microgrid. P_{Gas} is the input gas power. L_E, L_T, L_H and L_G denote the electric, thermal, hydrogen and gas loads in the microgrid, respectively. S_T is the heat storage device. S_H is the gas storage device. P_{fc}^E is the power supplied by the fuel cell, and P_{Gas}^M is the power supplied by the methanization unit.

The coupling matrix C for the energy transformation of the multi-energy microgrid is expressed as in equation (12):

$$C=\begin{bmatrix} k_1\sigma_1 & k_2\theta_1\beta_1\eta_e^{GT} \\ k_3\sigma_2\eta_t^{EB} & k_4\theta_1\eta_t^{RB}\beta_2\eta_t^{GT} \\ \left(k_5\omega_1+k_6\omega_2\right)\sigma_3\eta_h^{P2H} & 0 \\ 0 & k_7\theta_2 \end{bmatrix} \tag{12}$$

where σ denotes the distribution of distributed power sources and purchased and sold electricity in the microgrid. Where σ_1, σ_2 and σ_3 are the proportion of electric energy allocated to electric loads, electric boilers, and electric-to-hydrogen units, respectively. θ denotes the gas allocation in the microgrid. Where θ_1, θ_2 are the allocation ratios of gas turbine and gas load, respectively. β denotes the allocation of gas turbine energy supply. β_1, β_2 denote the proportion of gas for power and heat supply. η_e^{GT} is the efficiency of gas turbine power supply. η_t^{EB}, η_t^{RB} are the efficiency of electric boiler and waste heat boiler for heat supply. η_h^{P2H} is the electric hydrogen production efficiency, and ω_1, ω_2 are the electric energy allocation coefficients between hydrogen load and hydrogen storage equipment. k_1-k_9 are 0-1 decision parameters for individual microgrid types.

The power balance relationship for the hydrogen power conversion as well as the methanization unit is given in equation (13):

$$\begin{bmatrix} P_e^{FC} \\ 0 \\ 0 \\ P_{Gas}^M \end{bmatrix}=\begin{bmatrix} k_8\alpha_1\eta_e^{FC} \\ 0 \\ 0 \\ k_9\alpha_2\eta_g^M \end{bmatrix}\left[P_{H_2}^A\right] \tag{13}$$

where η_e^{FC} is the fuel cell power supply efficiency. η_g^M is the hydrogen methanation efficiency. α denotes the allocation of hydrogen energy in the hydrogen storage device, α_1, α_2 are the allocation ratio in the fuel cell and methanization device, respectively. $P_{H_2}^A$ is the hydrogen discharge power of the hydrogen storage device.

In the electric energy interaction between the multi-energy microgrid and the grid, ΔP_E in Eq. (8) is expressed as the difference between the input and output electric power of the microgrid, which can be used as an important embodiment of the microgrid to provide regulation for the grid, and ΔP_E can be expressed as Eq. (14):

$$\Delta P_E=P_{E,in}-P_{E,out} \tag{14}$$

where $P_{E,in}$ is the purchased electric power. $P_{E,out}$ is the outgoing electric power. When $\Delta P_E<0$ means that the microgrid sells power to fill the power deficit. When $\Delta P_E>0$, it means that the microgrid purchases power to consume the excess power.

II. B.Extraction of time-varying features of system inertia

In a power grid with a high proportion of new energy, the inertia level of the system has time-varying characteristics due to the stochastic and fluctuating nature of the new energy output, the new energy penetration rate in each time period, and the power generation and start-stop state of the synchronous generators, which are generally different.

In order to extract the time-varying characteristics of system inertia more comprehensively, this paper not only adopts the total rotational kinetic energy of the operating units to characterize the inertia level of the system in different time periods, but also proposes the rate of change of inertia index (RoCoI), which is used to analyze the impact of the actual scale of new energy access on the total inertia of the system in different time periods. The calculation formula for the rate of change of inertia is equation (15):

$$R_{oCoI} = \frac{dE_{sys}}{dR_{pen}} \tag{15}$$

where, R_{oCoI} is the inertia change rate. R_{pen} is the new energy penetration rate, which can be obtained from equation (16):

$$R_{pen} = \frac{\sum_{j=1}^{m} P_{Wj} \cdot x_{Wj}}{\sum_{i=1}^{n} P_{Gi} \cdot x_{Gi} + \sum_{j=1}^{m} P_{Wj} \cdot x_{Wj}} \tag{16}$$

where P_{Gi} and P_{Wj} denote the active power from synchronous generator i and new energy unit j respectively.

The inertia rate of change can be used to reveal the inertia deficit of the system, so as to prevent the system from falling into the ultra-low inertia operation state and lacking the ability to cope with large-capacity power disturbances. If the value of R_{oCoI} is much less than 0 during the gradual increase of the proportion of new energy grid connection, it indicates that the system inertia level may decline rapidly. If the value of R_{oCoI} is greater than the acceptable value, it can be considered that after the new energy unit is connected to the grid, the system inertia level will only have a small decrease, and the adaptability of the new energy unit access is good. It is worth noting that, in the case that the new energy penetration rate remains unchanged in the adjacent time period, while the total rotational kinetic energy of the system increases or decreases slightly, the inertia rate-of-change-time curve will have a singularity, and at this time, the time-varying characteristics of the system inertia can be extracted and screened by combining with the total rotational kinetic energy of system operating units, so as to judge the trend of the change of the system inertia level.

II. C.Methodology for assessing the external participation capacity of network partitions

Considering adjustable resource variability, geographic location, voltage level, etc., different network partitions will be formed within the NUPG (internal partitioned/gridded networks, distribution networks, micro-networks with larger capacity, etc.).The NUPG can issue scheduling commands to each network partition when needed, i.e., scheduling will be performed on the basis of the whole of the network partition as a unit. Each network partition is aggregated according to the response characteristics of the internal aggregation unit to obtain the excitation response characteristics of the network partition.

Taking partition k as an example, let there be m EBL aggregation units and n CACL aggregation units inside it, and the excitation-response extreme points of each aggregation unit are $\left(\gamma_{e1}^{e}, P_{e1}^{\max}\right)$, $\left(\gamma_{em}^{e}, P_{em}^{\max}\right)$ and $\left(\gamma_{cn}^{e}, P_{cn}^{\max}\right)$. Based on the excitation response characteristics and extreme points of each aggregated cell, they are aggregated to obtain the excitation response-characteristic curve $\Delta P_k^{Zup} = f_k\left(\gamma^{e}\right)$ of partition k as shown in Equation (17). The network partition k is based on the task ΔP_k^{δ} issued by NUPG, and based on this excitation-response characteristic curve $\Delta P_k^{\mathrm{Zup}} = f_k(\gamma^{\mathrm{c}})$, the excitation is given to the different internal aggregation units γ_{ke1}^{e}, γ_{kem}^{e} and γ_{kcn}^{e}, and the sum of the incentives is the total partition incentive $\gamma_{k\delta}^{e}$, as shown in equation (18). Each aggregation unit according to the issued incentive, based on the response characteristic curve to motivate the internal resources to participate in the response to complete their respective tasks ΔP_{ke1}^{δ}, ΔP_{kem}^{δ} and ΔP_{kcn}^{δ}, and ultimately complete the total task ΔP_k^{δ}, as shown in equation (19).

$$f_k\left(\gamma^e\right)=\begin{cases} f_{e1}^{eup}\left(\gamma^e\right)+\cdots+f_{em}^{eup}\left(\gamma^e\right)+\cdots+f_{cn}^{eup}\left(\gamma^e\right),\gamma^e<\gamma_{e1}^e \\ P_{e1}^{\max}+f_{e2}^{eup}\left(\gamma^e\right)+\cdots+f_{em}^{eup}\left(\gamma^e\right)+\cdots+f_{cn}^{eup}\left(\gamma^e\right),P_{e1}^{exc}<\gamma^e<\gamma_{e2}^e \\ \vdots \\ P_{e1}^{\max}+\cdots+P_{em}^{\max}+\cdots+P_{cn-1}^{\max}+f_{cn}^{cup}\left(\gamma^e\right),P_{cn-1}^{exc}<\gamma^e<\gamma_{c1}^e \\ P_{e1}^{\max}+\cdots+P_{em}^{\max}+P_{c1}^{\max}+\cdots+P_{en}^{\max},\gamma^e>\gamma_{cn}^e \end{cases} \tag{17}$$

$$\gamma_{k\delta}^e=\gamma_{ke1}^e+\cdots+\gamma_{kem}^e+\cdots+\gamma_{kcn}^e \tag{18}$$

$$\Delta P_k^\delta=\Delta P_{ke1}^\delta+\cdots+\Delta P_{kem}^\delta+\cdots+\Delta P_{kcn}^\delta \tag{19}$$

When NUPG gives a task ΔP_k^δ to a network partition k, it needs to grasp the partition's parametric capacity ΔP_k^{Zup}. Therefore, in this section, based on the aggregated unit parametric capability assessment method, we propose a multi-timescale net parametric capability assessment method for network partitions that can be externally provided based on the aggregation characteristics of the grid.

In general, each NUPG network partition first dispatches internal resources to solve its own internal problems, and then has spare capacity to support the external main network operation. At this time, some of the internal participation capacity has been consumed, and the capacity that can be provided externally to participate in the main network scheduling is reduced. Therefore, for the scheduling needs of network partitions and higher-level grids (NUPG and external main grid), this section mainly evaluates the net participation capacity that can be provided externally after the network partition has consumed part of its own participation capacity internally. However, when systematic problems occur in the main network: the internal resources of NUPG need to prioritize the support of external main network dispatching, and hand over the dispatching authority to the external main network for a short period of time, so as to assist the external main network in solving the systematic and global problems, and to ensure the stable operation of the system as a whole. At this time, NUPG can provide the external dispatching capacity without considering the internal consumption of all adjustable dispatching capacity.

First, an assessment method of online net parametric capacity that can be provided externally by the network partition is proposed as follows: taking into account the internal consumption of parametric capacity $\Delta P_k^{\xi up}(t,\Delta t)$ and $\Delta P_k^{\xi dn}(t,\Delta t)$ in the network partition and based on the aggregation unit's online parametric capacity assessment method to evaluate the external net parametric capacity of NUPG network partitions, as shown in equation (20). This method provides NUPG with network partitioned net parameterization capabilities that can be efficiently scheduled to enhance the effectiveness of NUPG scheduling.

$$\begin{cases} \Delta P_k^{Zup}(t,\Delta t)=\sum_{i=1}^{m}\Delta P_i^{eup}(t,\Delta t)+\sum_{j=1}^{n}\Delta P_j^{cup}(t,\Delta t)-\Delta P_k^{\xi up}(t,\Delta t) \\ \Delta P_k^{Zdn}(t,\Delta t)=\sum_{i=1}^{m}\Delta P_i^{edn}(t,\Delta t)+\sum_{j=1}^{n}\Delta P_j^{cdn}(t,\Delta t)-\Delta P_k^{xdn}(t,\Delta t) \end{cases} \tag{20}$$

Eq:

$\Delta P_k^{Zup}(t,\Delta t)$ - the externally available, on-line adjustable upward capacity (kW) of network partition k.

$\Delta P_k^{Zdn}(t,\Delta t)$ - the externally available, online down-adjustable capacity (kW) of network partition k.

$\Delta P_i^{eup}(t,\Delta t)$ - online upward adjustable capacity (kW) of EBL aggregation unit i.

$\Delta P_i^{edn}(t,\Delta t)$ - online downward adjustable capacity (kW) of EBL aggregation unit i.

$\Delta P_j^{cup}(t,\Delta t)$ - the online up-adjustable capacity (kW) of CACL aggregation unit j.

$\Delta P_j^{cdn}(t,\Delta t)$ - online down-adjustable capacity of CACL aggregation unit j (kW).

m - number of EBL aggregation units in partition k.

n - number of CACL aggregation units within partition k.

$\Delta P_k^{\xi up}(t,\Delta t)$ - the up-regulation capacity (kW) consumed by partition k to process internal tasks at moment t.

$\Delta P_k^{\xi dn}(t,\Delta t)$ - the down-regulation capacity (kW) consumed by partition k processing internal tasks at moment t.

The proposed method for assessing the sustained net parametric capacity that can be externally provided by the network partition is as follows: considering the up-regulation capacity $P_k^{\xi up}(t,\lambda t)$ and the down-regulation capacity $P_k^{\xi dn}(t,\lambda t)$ consumed by the network partition k itself, the method for assessing the sustained parametric capacity of the aggregation unit is as follows: assessing the NUPG network partitions can externally provide the sustained net parametric regulation capacity, as shown in Eqs. (21) and (22), to provide support for NUPG online imbalance scheduling.

$$\begin{cases} P_{k\lambda}^{up}(t,\lambda t) = P_{z\lambda}^{up}(t,\lambda t) + P_{zr}^{up}(t,\lambda t) - P_k^{\xi up}(t,\lambda t) \\ P_{k\lambda}^{dn}(t,\lambda t) = P_{z\lambda}^{dn}(t,\lambda t) + P_{zr}^{dn}(t,\lambda t) - P_k^{\xi dn}(t,\lambda t) \end{cases} \tag{21}$$

$$\begin{cases} \lambda t = f_k^{up}(P_{k\lambda}^{up}(t,\lambda t)) \\ \lambda t = f_k^{dn}(P_{k\lambda}^{dn}(t,\lambda t)) \end{cases} \tag{22}$$

Eq:

$P_{k\lambda}^{\mathrm{up}}(t,\lambda t)$ - the upward capacity (kW) of the network partition k that can be available outside the partition for a continuous λt duration at time t after processing internal tasks.

$P_{k\lambda}^{\mathrm{dn}}(t,\lambda t)$ - The network partition k can provide continuous λt hours of downward capacity (kW) outside the partition at time t after processing internal tasks.

$f_k^{up}(P_{k\lambda}^{up}(t,\lambda t))$ - Function of sustained upward capacity that network partition k can provide externally.

$f_k^{dn}(P_{k\lambda}^{dn}(t,\lambda t))$ - the sustained down-regulation capacity function externally available to network partition k.

Then, the intraday net parametric capacity assessment method that can be externally provided by the network partition is proposed in the following steps: consider the up-regulation capacity $\Delta P_k^{\xi up}(nT,\Delta t)$ and the down-regulation capacity $\Delta P_k^{\xi dn}(nT,\Delta t)$ consumed by the network partition k itself based on the aggregation of the unit intraday participation capacity assessment method to assess the net intraday participation capacity that can be externally provided by the NUPG network partition, as shown in Equation (23), which can provide support for NUPG in intraday imbalance scheduling.

$$\begin{cases} \Delta P_k^{Zup}(nT,\Delta t) = \sum_{i=1}^{m} \Delta P_i^{eup}(nT,\Delta t) + \sum_{j=1}^{n} \Delta P_j^{cup}(nT,\Delta t) \\ \qquad\qquad -\Delta P_k^{\xi up}(nT,\Delta t) \\ \Delta P_k^{Zdn}(nT,\Delta t) = \sum_{i=1}^{m} \Delta P_i^{edn}(nT,\Delta t) + \sum_{j=1}^{n} \Delta P_j^{cdn}(nT,\Delta t) \\ \qquad\qquad -\Delta P_k^{\xi dn}(nT,\Delta t) \end{cases} \tag{23}$$

Eq:

$\Delta P_k^{Zup}(nT,\Delta t)$ - the upward capacity (kW) that network partition k can provide externally during the day.

$\Delta P_k^{Zdn}(nT,\Delta t)$ - the downward capacity (kW) that network partition k can externally provide during the day.

$\Delta P_i^{eup}(nT,\Delta t)$ - Intraday up-regulation capacity (kW) available to EBL aggregation unit i.

$\Delta P_i^{edn}(nT,\Delta t)$ - Intraday downward capacity of EBL aggregation unit i (kW).

$\Delta P_j^{cup}(nT,\Delta t)$ - Intraday upward capacity (kW) of CACL aggregation unit j.

$\Delta P_j^{cdn}(nT,\Delta t)$ - Intraday downward capacity of CACL aggregation unit j (kW).

$\Delta P_k^{\xi up}(nT,\Delta t)$ - Intraday up-regulation capacity (kW) consumed by partition k for processing internal tasks.

$\Delta P_k^{\xi dn}(nT,\Delta t)$ - the intraday downward capacity (kW) of partition k to handle internal task consumption.

Finally, a day-ahead net parameterization capacity assessment method that can be provided externally by the network partition is proposed in the following steps: considering the upward parameterization capacity $\Delta P_k^{\xi up}(t)$ and the downward parameterization capacity $\Delta P_k^{\xi dn}(t)$ reserved for processing internal tasks, the day-ahead parameterization capacity assessment method based on the aggregation unit evaluates the NUPG network partition's day-ahead net external parameterization capability, as shown in Eq. (24), which can improve the quality of NUPG day-ahead operation plan development.

$$\begin{cases} \Delta P_k^{Zup}(t) = \sum_{i=1}^{m} \Delta P_i^{eup}(t) + \sum_{j=1}^{n} \Delta P_j^{cup}(t) - \Delta P_k^{\xi up}(t) \\ \Delta P_k^{Zdn}(t) = \sum_{i=1}^{m} \Delta P_i^{edn}(t) + \sum_{j=1}^{n} \Delta P_j^{cdn}(t) - \Delta P_k^{\xi dn}(t) \end{cases} \quad (24)$$

Eq:

$\Delta P_k^{Zup}(t)$ - the day-ahead externally available uprating capacity (kW) that network partition k can provide.

$\Delta P_k^{Zdn}(t)$ - the day-ahead down-adjustable capacity (kW) that network partition k can externally provide.

$\Delta P_i^{eup}(t)$ - the day-ahead up-adjustable capacity (kW) of EBL aggregation unit i.

$\Delta P_i^{edn}(t)$ - the day-ahead downward adjustable capacity (kW) of EBL aggregation unit i.

$\Delta P_j^{cup}(t)$ - the day-ahead up-adjustable capacity (kW) of CACL aggregation unit j.

$\Delta P_j^{cdn}(t)$ - the day-ahead down-adjustable capacity (kW) of CACL aggregation unit j.

$\Delta P_k^{\xi up}(t)$ - the day-ahead up-adjustable capacity (kW) of network partition k reserved to handle internal tasks.

$\Delta P_k^{\xi dn}(t)$ - network partition k reserved to handle internal tasks with day-ahead downward capacity (kW).

III. Application and optimization of supply and demand risk adjustment capacity assessment methods

III. A. Application analysis

III. A. 1) Validation of key indicators of adjustable load regulation capability

From November 31 to December 5, 2021, the Southwest Branch of China Power Grid conducted a total of six upper and lower power regulation control tests on an electric vehicle charging station in a certain city across provinces. Now, Charging Station 1(EVCSI) and Charging Station 2(EVCS2) are selected to evaluate four indicators: control deviation rate, control delay duration, control delay rate, and control success rate. The power change curves of EVCS1 and EVCS2 participating in six grid regulation tests are shown in Figures 2 and 3 respectively. In the process of EVCS1 participating in power grid regulation, the time points of 13:00:35, 13:01:45, 13:02:55, 13:04:05, 13:05:15 and 13:06:25 correspond respectively to: Down-regulation test 1 instruction issued, up-regulation test 1 instruction issued, down-regulation test 2 instruction issued, up-regulation test 2 instruction issued, down-regulation test 3 instruction issued, up-regulation test 3 instruction issued. In the process of EVCS2 participating in power grid regulation, the time points of 13:00:00, 13:01:10, 13:02:20, 13:03:30, 13:04:40 and 13:05:50 correspond respectively to: Down-regulation test 1 instruction issued, up-regulation test 1 instruction issued, down-regulation test 2 instruction issued, up-regulation test 2 instruction issued, down-regulation test 3 instruction issued, up-regulation test 3 instruction issued.

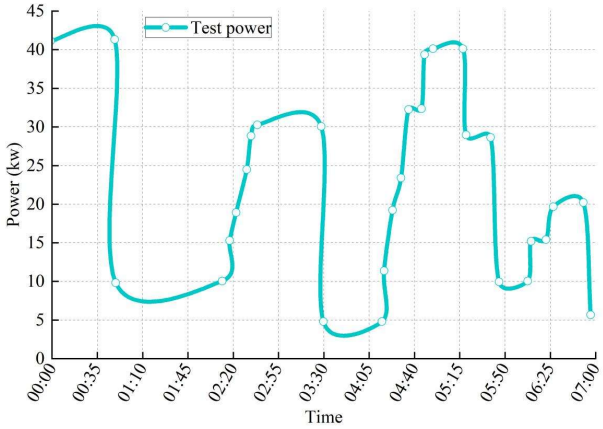

Figure 2: Power curve of regulation control test for EVCS1(13:00)

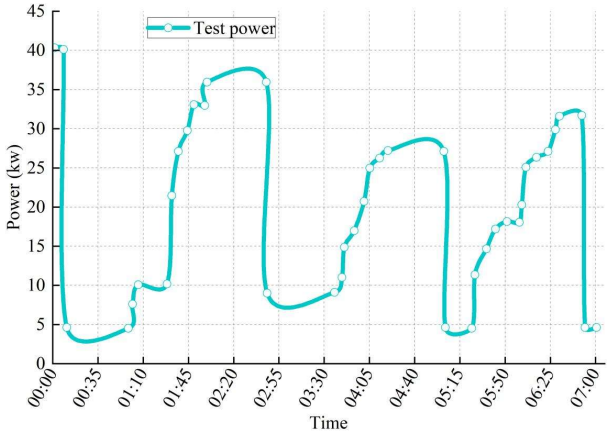

Figure 3: Power curve of regulation control test for EVCS2(13:00)

When the power up-regulation test, there is an obvious slow climbing phenomenon, the response time is longer, between 35~95s. Charging station 1 upregulation time is obviously shorter than charging station 2, the root cause is the rate of climb and the initial capacity of the battery is related to the battery, the lower the battery capacity is the faster the upregulation speed, charging station 1 than charging station 2 battery initial capacity is low, indicating that the 2 charging station regulating response capacity are equipped to participate in the peak shifting and frequency regulation market.

III. A. 2) Trend analysis of electricity load

Extracting the local March-July electricity load data of the object of analysis in the previous section, 1 day is divided into 24 time points, and the extracted load data is shown in Fig. 4.

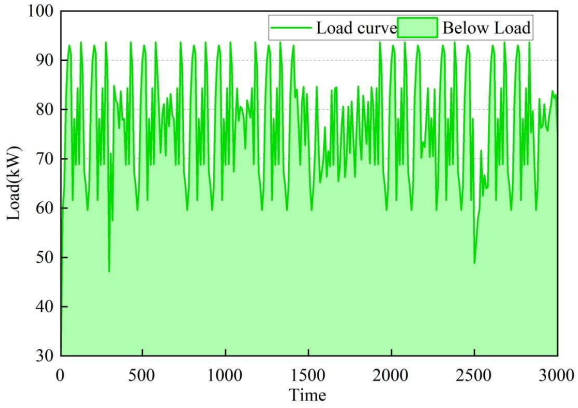

Figure 4: Local power load data from March to July

As can be seen from the figure, the electrical load in the region is maintained between 60-100 kW in the March-July time period and there are distinctive features of the forecast curve. It is mainly reflected in the following aspects:

(1) Periodicity: the electric load curve in this region not only exists in daily periodicity, but also in a period of time. First of all the cyclical fluctuation within the day mainly exists in the change of electricity consumption during the day and at night. During the daytime, people usually need more supply of electricity to fulfill their work requirements and living needs. At night, people's demand for electricity then decreases, and this cyclical fluctuation comes from the transformation of people's life style, work style, and production activities within a day.

(2) Non-linearity: as can be seen from the figure, the load curve of the power system shows a complex non-linear relationship. This may be due on the one hand to the operating characteristics of certain power equipment is itself non-linear, the power consumption of these power equipment and the size of the load between the state of operation is not just a simple linear relationship.

(3) Fluctuation (randomness): From the figure, it can be clearly seen that there is a certain degree of randomness in the load curve, and unexpected events (such as natural disasters, equipment failures) or

abnormalities (such as power outages, insufficient power supply, etc.) will lead to fluctuations in the load curve of the power system.

III. B. Optimization of microgrid potential regulation capacity assessment

III. B. 1) Analysis of the regulation capacity of energy storage units

The curve $R_{\alpha R}(\beta)$ of the power output from the energy storage unit is shown in Fig. 5.

In the next cycle, the total amount of power that needs to be absorbed (charged) by the energy storage unit is the risk reserve power $E_{R\alpha R}$ i.e., the area on the straight line: y=0 in Fig. 5, S1. The total amount of power that needs to be output (discharged) by the energy storage unit is the risk deficit power $E_{L\alpha R}$ i.e., the area on the straight line: y=0 in Fig. 5, S2.

If the energy storage unit outputs power of ΔE in the next cycle, it is equivalent to the system reserve capacity $\bar{R}$ increases $\Delta E/T$, i.e., the risk reserve $R_{\alpha R}(\beta)$ curve is shifted upward $P=\Delta E/T$. Obviously, the risky reserve power $E_{R\alpha R}=S_1$ of the regulated microgrid increases, and the risky deficit power $E_{R\alpha R}=S_2$ decreases.

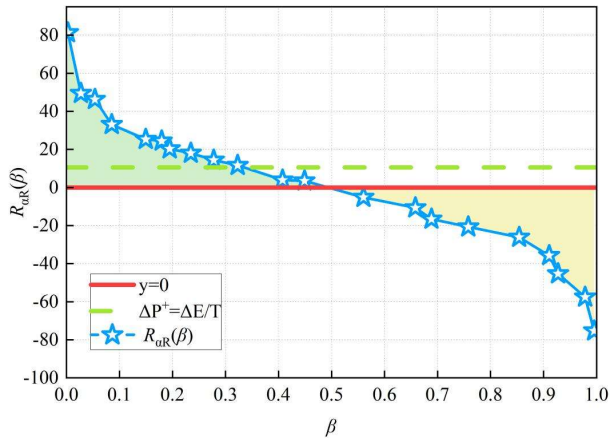

Figure 5: The output power curve of the energy storage unit

The risk back-up curve $R_{\alpha R}(\beta)$ for power absorption by the energy storage unit is shown in Figure 6.

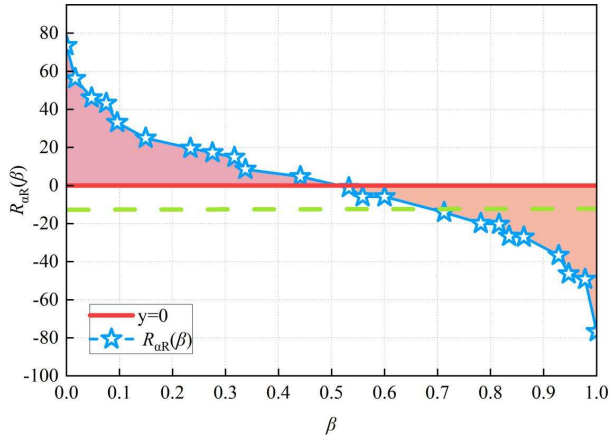

Figure 6: The risk-reserve curve for energy storage units to absorb electrical energy

If the energy storage unit absorbs power in the next cycle as ΔE, it is equivalent to the system reserve capacity $\bar{R}$ decreases by $\Delta E_c/T$, i.e., the risk-standby $R_{\alpha R}(\beta)$ curve is shifted downward $P^0=\Delta E_c/T$. Obviously, the risky reserve power $E_{R\alpha R}$ of the microgrid decreases and the risky deficit power $E_{R\alpha R}$ increases after regulation.

As long as the microgrid has sufficient storable power (space) and stored power at the moment of t, by controlling the amount of charging/discharging of the energy storage units in real time, the overall amount of risky power that can be automatically smoothed out during the dispatch cycle is $\min\{E_{R\alpha R}, E_{L\alpha R}\}$. If $E_{R\alpha R}>E_{L\alpha R}$, the

remaining power needs to be deposited into the energy storage unit, so that the amount of power stored at the moment of $t+T$ increases. If $E_{R\alpha R} < E_{L\alpha R}$ insufficient power is the power that needs to be output by the energy storage unit in that cycle, making the power storage at the $t+T$ moment decrease. Therefore, the imbalance risk power is as in equation (25):

$$\Delta E = E_{R\alpha R} - E_{L\alpha R} \tag{25}$$

Its positive and negative should be made as the boundary line of state space division.

Secondly, in the next dispatch period T, the energy storage situation and the remaining storage space of the energy storage unit also directly affect the regulation capability. When $\Delta E > 0$, it means that there is a surplus of power generation during the dispatch period, so whether the energy storage unit can absorb the excess risk reserve power should be the primary issue. On the other hand, when $\Delta E < 0$, it means that there is insufficient power generation during the dispatch period, and the primary question is whether the stored power can meet the load demand during the dispatch period. So the adequacy of the stored power and the storage space should also be the boundary line of state division.

III. B. 2) Simulation experiments

The theoretical calculation and simulated operation simulation results of the potential regulation capacity of this microgrid during the dispatch period are shown in Table 1, where V1: theoretical value, V2: simulated value, V3: difference = theoretical value - simulated value. The evaluation indexes of the microgrid's external source/carrier regulation capability are: outputable power (Eout), inputable power (Ein), and the internal operation evaluation power: maximum abandoned power (Eg), maximum load shedding power (EL).

Table 1: The calculation and simulation results of the regulation capacity assessment

	Eout			Ein			Eg			EL		
No	V1	V2	V3	V1	V2	V3	V1	V2	V3	V1	V2	V3
1	27.6	27.6	0	17.6	17.6	0	0	0	0	0	0	0
2	11	11	0	31.2	34.2	-3	0	0	0	3	0	3
3	36.7	44.7	-8	0.4	1.9	-1.5	8.2	1.6	6.6	0	0	0
4	20.7	28.4	-7.7	16.4	16.8	-0.4	7.8	0	7.8	0.5	0	0.5
5	38.4	47.8	-9.4	0	0	0	12.1	27.1	-15	0	0	0
6	44.1	45.5	-1.4	0	0	0	1.8	0.5	1.3	0.9	0	0.9
7	18.8	18.8	0	26.4	26.4	0	0	0	0	0	0	0
8	38	42.5	-4.5	2.7	2.8	-0.1	4.5	0.2	4.3	0	0	0
9	0.2	2.5	-2.3	32.2	45	-12.8	0	0	0	12.9	2.5	10.4
10	17	18.1	-1.1	23	27	-4	1.2	0	1.2	4.1	0	4.1
11	0	0	0	30.2	45.6	-15.4	0	0	0	4	0.6	3.4
12	0	0	0	36.7	45.1	-8.4	2.5	0	2.5	8.6	0.2	8.4

The difference between the theoretically calculated values and simulation results of the microgrid's assessment indicators of external source/load regulation capability of exportable power (Eout) and importable power (Ein) is not significant and both are less than or equal to 0.00 as a negative value, verifying that the theoretical value is that the microgrid can ensure the provision or absorption of power externally in the next cycle.

The difference between the theoretical calculated value and the simulation result of the evaluation indexes of internal operation, the maximum energy-generating capacity (Eg) and the maximum load-shedding capacity (EL), is positive, which verifies that the theoretical value can indicate whether the microgrid has energy-generating or load-shedding phenomenon in the next cycle and how the most serious situation is.

In practical application, if the microgrid is in grid-connected state, the two evaluation indexes of its external regulation capability can be used as the most basic output or input capability of the microgrid when the higher-level dispatching department conducts the peak shaving and valley filling scheduling. The inevitable realization of peak shaving and valley filling during the dispatch period can be guaranteed. Similarly, in the islanding state, the two assessment indicators of the internal operation of the microgrid can be used as the microgrid operation scheduling to make the worst preparation for the operation state in the next scheduling cycle to ensure the normal and reliable operation of the microgrid.

IV. Conclusion

In this paper, a multi-energy microgrid power regulation model is proposed to characterize the energy conversion and input-output relationship between energy sources in the grid system. At the same time, an inertia change rate index is designed to obtain the spatial and temporal distribution characteristics of the inertia of the grid system and to identify the time-varying characteristics of the grid system. By calculating the multi-dimensional spatial and temporal trends of the grid system and combining with the assessment method of the network partition's external participation capacity, the assessment of the supply and demand risk adjustment capacity of provincial grids with a high proportion of new energy is realized.

The designed assessment method defines four indicators for the assessment of potential regulation capability of microgrids in the simulation experiment of microgrid potential regulation capability assessment from the perspectives of both external source/load regulation capability and internal operation: outputable power (Eout), inputable power (Ein), maximum energy-generating capacity (Eg), and maximum load-shedding capacity (EL). Among them, the difference between the theoretical and simulated values of the external source/load regulation assessment indexes (Eout, Ein) is less than or equal to 0.00, which verifies that the theoretical value is that the microgrid can ensure that power can be provided or absorbed externally in the next cycle. The difference between the theoretical and simulated values of the internal operation assessment metrics (Eg, EL) is greater than or equal to 0.00, which verifies that the theoretical values can indicate whether or not energy abandonment or load shedding occurs in the microgrid in the next cycle and what the worst case scenario is.

Funding

This research was supported by the State Grid Headquarters Project: Key Technologies and Applications for Supply-Demand Risk Identification and Planning Decision Simulation of Provincial Power Grids with High Penetration of Renewable Energy (1400-202324646A-3-2-ZN).

References

[1] Yao, J., Wang, X., Xing, L., Chang, Y., Li, Z., Sun, T., & Fan, M. (2022, December). New Electricity Market Mechanism for High Proportion of New Energy. In 2022 2nd International Conference on Electrical Engineering and Control Science (IC2ECS) (pp. 492-495). IEEE.

[2] Xu, B., & Lin, B. (2018). Assessing the development of China's new energy industry. Energy Economics, 70, 116-131.

[3] Zhang, D., Wang, J., Lin, Y., Si, Y., Huang, C., Yang, J., ... & Li, W. (2017). Present situation and future prospect of renewable energy in China. Renewable and Sustainable Energy Reviews, 76, 865-871.

[4] Liu, G., Dou, D., Wang, Y., Li, X., Gao, Z., & Lv, H. (2024). Multi-scenario flexibility requirement analysis of high proportion of new energy access to power system. Clean Energy, 8(6), 187-204.

[5] Pan, Y., & Dong, F. (2022). Dynamic evolution and driving factors of new energy development: Fresh evidence from China. Technological Forecasting and Social Change, 176, 121475.

[6] Xu, B., & Lin, B. (2018). Do we really understand the development of China's new energy industry?. Energy economics, 74, 733-745.

[7] Xu, Q., Li, W., Yin, B., Wang, X., Wang, X., & Xu, M. (2024, December). Research on Influencing Factors and Decision-Making of Power Transmission of High Proportion New Energy Power Grid. In 2024 Boao New Power System International Forum-Power System and New Energy Technology Innovation Forum (NPSIF) (pp. 139-145). IEEE.

[8] Linlin, Y., Lihua, Z., Gaojun, M., Feng, Z., & Wanxun, L. (2022). Research on multi-objective reactive power optimization of power grid with high proportion of new energy. IEEE Access, 10, 116443-116452.

[9] Song, J., Zhou, X., Zhou, Z., Wang, Y., Wang, Y., & Wang, X. (2023). Review of low inertia in power systems caused by high proportion of renewable energy grid integration. Energies, 16(16), 6042.

[10] Hongbo, L. I. U., Shencheng, L. I. U., Xueyang, G. A. I., Yongfa, L. I. U., & Yutong, Y. A. N. (2024). Overview of Active Distribution Network Planning With High Proportion of New Energy Access. Power Generation Technology, 45(1), 151.

[11] Liu, T., Song, Y., Zhu, L., & Hill, D. J. (2022). Stability and control of power grids. Annual review of control, robotics, and autonomous systems, 5(1), 689-716.

[12] Shair, J., Li, H., Hu, J., & Xie, X. (2021). Power system stability issues, classifications and research prospects in the context of high-penetration of renewables and power electronics. Renewable and Sustainable Energy Reviews, 145, 111111.

[13] Ahmed, F., Al Kez, D., McLoone, S., Best, R. J., Cameron, C., & Foley, A. (2023). Dynamic grid stability in low carbon power systems with minimum inertia. Renewable Energy, 210, 486-506.

[14] Khan, S. A., Wang, M., Su, W., Liu, G., & Chaturvedi, S. (2022). Grid-forming converters for stability issues in future power grids. Energies, 15(14), 4937.

[15] Wang, C., Yuan, C., Xie, D., Zhang, Z., Zhang, X., & Li, T. (2022, September). Research on energy storage scheduling strategy considering high proportion of new energy uncertainty. In 2022 5th International Conference on Renewable Energy and Power Engineering (REPE) (pp. 417-421). IEEE.

[16] Gong, L., Cao, W., Liu, K., Yu, Y., & Zhao, J. (2020). Demand responsive charging strategy of electric vehicles to mitigate the volatility of renewable energy sources. Renewable Energy, 156, 665-676.

[17] Qu, H., Duan, Q., & Niu, M. (2018). Modeling the volatility of realized volatility to improve volatility forecasts in electricity markets. Energy Economics, 74, 767-776.

[18] Staffell, I., & Pfenninger, S. (2018). The increasing impact of weather on electricity supply and demand. Energy, 145, 65-78.

[19] Hosseinzadeh, N., Aziz, A., Mahmud, A., Gargoom, A., & Rabbani, M. (2021). Voltage stability of power systems with renewable-energy inverter-based generators: A review. Electronics, 10(2), 115.

[20] Liang, X. (2016). Emerging power quality challenges due to integration of renewable energy sources. IEEE Transactions on Industry Applications, 53(2), 855-866.
[21] Zhang, H., Xiang, W., Lin, W., & Wen, J. (2021). Grid forming converters in renewable energy sources dominated power grid: Control strategy, stability, application, and challenges. Journal of modern power systems and clean energy, 9(6), 1239-1256.
[22] Meegahapola, L., Sguarezi, A., Bryant, J. S., Gu, M., Conde D, E. R., & Cunha, R. B. (2020). Power system stability with power-electronic converter interfaced renewable power generation: Present issues and future trends. Energies, 13(13), 3441.
[23] Liu, D. N. (2015). Model for evaluating the electrical power system safety with hesitant fuzzy linguistic information. Journal of Intelligent & Fuzzy Systems, 29(2), 725-730.
[24] Oyewole, P. A., & Jayaweera, D. (2020). Power system security with cyber-physical power system operation. IEEE Access, 8, 179970-179982.
[25] Deane, J. P., Gracceva, F., Chiodi, A., Gargiulo, M., & Gallachoir, B. P. (2015). Assessing power system security. A framework and a multi model approach. International Journal of Electrical Power & Energy Systems, 73, 283-297.